Preferred site occupation of 3d atoms in NixFe4−xN(x=1 and 3) films revealed by x-ray absorption spectroscopy and magnetic circular dichroism

著者	Takata Fumiya, Ito Keita, Takeda Yukiharu, Saitoh Yuji, Takanashi Koki, Kimura Akio, Suemasu Takashi
journal or publication title	Physical review materials
volume	2
number	2
page range	024407
year	2018-02
権利	(C)2018 American Physical Society
URL	http://hdl.handle.net/2241/00152963

doi: 10.1103/PhysRevMaterials.2.024407

Preferred site occupation of 3*d* atoms in $Ni_xFe_{4-x}N$ (x = 1 and 3) films revealed by x-ray absorption spectroscopy and magnetic circular dichroism

Fumiya Takata[1], Keita Ito[2,3,*], Yukiharu Takeda[4], Yuji Saitoh[4], Koki Takanashi[2,3], Akio Kimura[5], and Takashi Suemasu[1,†]

[1] *Institute of Applied Physics, Graduate School of Pure and Applied Sciences, University of Tsukuba, Tsukuba, Ibaraki 305-8573, Japan*

[2] *Institute for Materials Research, Tohoku University, Sendai 980-8577, Japan*

[3] *Center for Spintronics Research Network, Tohoku University, Sendai 980-8577, Japan*

[4] *Condensed Matter Science Division, Japan Atomic Energy Agency (JAEA), Sayo, Hyogo 679-5148, Japan*

[5] *Graduate School of Science, Hiroshima University, Higashi-Hiroshima, Hiroshima 739-8526, Japan*

[*]itok@imr.tohoku.ac.jp

[†]suemasu@bk.tsukuba.ac.jp

X-ray absorption spectroscopy (XAS) and x-ray magnetic circular dichroism (XMCD) measurements were performed at the Ni and Fe $L_{2,3}$ and N K absorption edges for $Ni_xFe_{4-x}N$ (x = 1 and 3) epitaxial films. Spectral lineshape analysis and element-specific magnetic moment evaluations are presented. Shoulders at approximately 2 eV above the Ni $L_{2,3}$ main peaks in the XAS spectrum of Ni_3FeN, were interpreted to originate from hybridization of orbitals between Ni 3d at face-centered (II) sites and N 2p at body-centered sites, while such features were missing in $NiFe_3N$ film. Similar shoulders were observed at Fe $L_{2,3}$-edges in both films. These results indicate that the orbitals of Ni atoms did not hybridize with those of N atoms in the $NiFe_3N$ film. Hence, Ni atoms preferentially occupied corner (I) sites, where the hybridization was weak because of the relatively long distance between Ni at I sites and N atoms. The relatively large magnetic moment deduced from sum-rule analysis of $NiFe_3N$ also showed a good agreement with the presence of Ni atoms at I sites. Besides, the appearance of XMCD signal at the N K-edges implied that a magnetic moment was induced at the N atom owing to hybridization between the metal 3d and N 2p orbitals.

I. INTRODUCTION

Antiperovskite-type 3*d* transition metal nitrides have been extensively studied owing to their rich magnetic and electrical transport properties, which promote applications in magnetic and spintronics devices requiring low-power consumption and high-speed information transfer. These nitrides feature a face-centered cubic 3*d* transition metal lattice, in which one N atom is positioned at the body center of a face-centered cubic lattice composed of the transition metal. Here, we define the corner and face-centered atomic sites as I and II, respectively. The II sites are further divided into IIA and IIB sites in the presence of magnetization (arrow in Fig. 1). Among these materials, Fe_4N is most promising for spintronic device applications because of the theoretically expected negative high spin polarization of electrical conductivity ($P_\sigma = -1.0$) ascribed to a mixing between the orbitals of Fe 4*sp* at II sites and N 2*sp* [1]. The high spin polarization of Fe_4N has later been demonstrated via point contact Andreev reflection technique ($|P_\sigma| = 0.59$) [2], and tunneling magnetoresistance effect of −75% in magnetic tunnel junctions with Fe_4N electrode [3]. Substitution of other 3*d* transition metal atoms for Fe in Fe_4N is an effective means to modify their magnetic and transport properties. For instance, Co_3FeN, which is isostructural with Fe_4N, is theoretically predicted to show a larger negative spin polarization of the density of states (P_D) at the Fermi level (E_F) compared to Fe_4N [4].

Hence, a numerous number of studies have been conducted in this regard [5-8]. For another example, $Ni_xFe_{4-x}N$ has been widely investigated from the viewpoint of improving chemical stability and mechanical ductility inherent in Fe_4N, and modulating its electronic and magnetic properties [9-20]. There have been several reports on the fabrication of $Ni_xFe_{4-x}N$ ($0 \leq x \leq 4$) films and powders [11-15,20]. The substitution of Ni for Fe atoms tends to reduce the magnetic moment and shorten the lattice constants [13,20] Negative anisotropic magnetoresistance observed in Ni_3FeN and $NiFe_3N$ films is interpreted by both negative P_σ and P_D in those nitrides as is the case in Fe_4N [21,22]. Furthermore, the first-principles calculation predicts that Ni_3FeN has a larger $|P_D|$ of 0.86 ($P_D < 0$) than that of Fe_4N ($P_D = -0.49$). It can thus be nominated as a strong candidate of high spin-polarized material [20]. However, it is also theoretically pointed out that P_D is quite sensitive to the site occupation of 3*d* atoms in the lattice; a large $|P_D|$ is expected in $(Fe)^{I}(Ni)^{IIA,IIB}(N)$ configurations, where Fe atoms occupy I sites and Ni atoms are positioned at IIA and IIB sites, while $|P_D|$ decreases sharply ($P_D = -0.53$) for the $(Fe)^{IIB}(Ni)^{I,IIA}(N)$ configuration [20]. Therefore, it is important to know the actual preferred site occupation of 3*d* atoms in $Ni_xFe_{4-x}N$.

X-ray absorption spectroscopy (XAS) and x-ray magnetic circular dichroism (XMCD) measurements are powerful techniques for clarifying the element-specific

electronic structures of materials. Several XAS and XMCD studies of Fe_4N, Co_3FeN, and Co_4N films have so far been performed to investigate their local electronic states and magnetic moment [23-26]. The spectral lineshape analysis of the XAS and XMCD spectra obtained for Fe_4N has allowed us to conclude that the observed shoulders at the Fe $L_{2,3}$ main peaks can be explained by orbital hybridization between Fe 3*d* at II sites and the N 2*p* orbital [25]. Similar shoulders have been observed at the Co $L_{2,3}$-edges in Co_4N films, indicating that 3*d* orbitals of Co atoms at II sites hybridize with the N 2*p* orbital. Hence, these shoulders represent that 3*d* transition metals occupy II sites. In this work, we performed XAS and XMCD measurements of $Ni_xFe_{4-x}N$ (x = 1 and 3) films and evaluated the preferred site occupation of Ni and Fe atoms by analyzing the spectral shapes and magnetic moment.

II. EXPERIMENTAL

Ni_3FeN and $NiFe_3N$ films, 50-nm-thick, were epitaxially grown on a $SrTiO_3$(001) single-crystal substrate at a substrate temperature of 300 and 550 °C, respectively, by molecular beam epitaxy equipped with a radio frequency N plasma source and high temperature Knudsen cells as Fe and Ni sources. The growth details have been reported previously [20]. After the growth, a 3-nm-thick Al capping layer was

deposited *in situ* to prevent oxidation. XAS and XMCD measurements were performed at the twin helical undulator beamline BL23SU of SPring-8 in Japan [27]. Both the magnetic field of ±4 T and circularly polarized x-rays with almost complete left- and right- circular polarization were applied perpendicular to the film plane. The polarization of x-ray was switched at every energy point with a frequency of 1 Hz by using five kicker magnets which realize excellent signal-to-noise ratio (below 0.01%). The spectra were acquired in a total electron yield mode at the Ni and Fe $L_{2,3}$, and N K absorption edges, at 100 K. The external magnetic field of 4 T was found to be sufficient to saturate the sample magnetization.

III. RESULTS AND DISCUSSION

We first show the XAS and XMCD spectra at the Ni $L_{2,3}$-edges of Ni_3FeN and $NiFe_3N$ films in Figs. 2(a) and 2(b), respectively. There are variety of features in the XAS spectrum of both films. A distinct shoulder appears in the XAS spectrum of Ni_3FeN at 2 eV higher photon energy ($h\nu$) than those of the L_3 ($h\nu$ = 852 eV) and L_2 (869 eV) edges as denoted with arrows in Fig. 2(a). Another satellite with small spectral weight is found around 7 eV higher $h\nu$ than the main L_3 peak as marked with A. The corresponding satellite for the L_2 main edge is also recognizable (A'). The XAS spectrum of $NiFe_3N$ can

be distinguished from that of Ni_3FeN. Here, we notice that the intensities of the 2-eV shoulders observed for the Ni-rich film are substantially suppressed in the Fe-rich film, while the weak satellites A and A' remain almost unchanged as recognized in the upper part of Fig. 2(b). The XMCD spectra of these films also show a little complexity. In addition to the prominent negative and positive features at L_3 and L_2 main edges, we can see the satellites located 4 eV higher than those of respective main edges with the same signs as denoted with B and B' as shown in the lower part of Figs. 2(a) and 2(b). The main XMCD feature at both L_3- and L_2-edges for the Ni-rich film are a little broader than that for the Fe-rich sample. We notice that the satellite features B and B' are almost identical between the two films.

We now discuss the site occupations with the 2-eV shoulders in the XAS spectra of Ni_3FeN and $NiFe_3N$ films. Similar shoulders are also reported for Fe_4N and Co_4N films at the Fe and Co $L_{2,3}$-edges. These shoulders are typically observed in antiperovskite-type ferromagnetic nitrides [23-26], which are attributed to the electric dipole transition from a metal 2*p* core-level to a hybridization state generated between the orbitals of N 2*p* and metal 3*d* at II sites. Thus, the presence of the 2-eV shoulders in the XAS spectrum (arrows) of Ni_3FeN in Fig. 2(a) indicate that Ni atoms at II sites hybridize with the N atom. On the other hand, the absence of such shoulders can lead to

an explanation that the Ni atoms in the $NiFe_3N$ film are more likely to occupy I sites than II sites. From these results, it seems right to infer that Ni atoms in $Ni_xFe_{4-x}N$ firstly substitute Fe atoms at I site and subsequently replace them at II site with increasing Ni content. This tendency is in a good agreement with the results obtained from Mössbauer measurements and the first-principles calculations in terms of the configuration-dependent total energy [12,19]. This is also consistent with the narrow XMCD spectrum of $NiFe_3N$ in comparison with that of Ni_3FeN. That is, the strong Ni II *d*-N *p* hybridization broadens the spectrum, while this effect is missing for $NiFe_3N$ due to the absence of Ni atoms at II sites. It should be noted again that additional satellite features in the XAS (A, A') and the XMCD spectra (B, B') are commonly observed for both films. It is reminded that such characteristic features take place also in the elemental Ni crystal, where the satellites in Ni $L_{2,3}$ XAS and XMCD spectra appear at different photon energies [28]. The satellites of A and A' in XAS spectra can be reproduced by one-electron relativistic tight-binding calculation, but the B and B' satellites in XMCD were not appeared in that model [29]. It was reasonably interpreted that those satellites in XAS and XMCD were due to the configurations interaction between the final state multiples described with $2p^53d^9$ and $2p^53d^{10}$ [30]. Having considered this aspect, we can safely interpret that the 2-eV shoulders in the Ni-$L_{2,3}$ XAS spectrum and commonly observed

satellites labeled as A (A') and B (B') at L_3- (L_2-) edges comes from different origins. The former is mainly due to the unoccupied states derived from Ni II *d*-N 2*p* hybridization contributed from the Ni atoms at II site solely, on the other hand, the latter stems from the electron correlation effect which is not necessarily related to the site occupation of the Ni atoms.

Figures 3(a) and 3(b) show the circularly polarized Fe $L_{2,3}$-edges XAS and XMCD spectra in Ni_3FeN and $NiFe_3N$ films, respectively. In addition to the main XAS peaks at 707.3 eV and 720.5 eV for the Fe L_3- and L_2-edges, respectively, shoulders are observed at approximately 2 eV higher than that of each main peak, as denoted with arrows in Fig. 3. The almost identical satellite features of Fe $L_{2,3}$-edge XAS spectra of Ni_3FeN and $NiFe_3N$ tells us that Fe atoms in both films occupy only II sites. It is also consistent with the above-mentioned consideration for $NiFe_3N$ that the I sites are almost occupied by Ni atoms. The XMCD spectra of both samples show negative and positive features at Fe L_3- and L_2-edges, respectively. The same sign of the XMCD signal signifies that the Fe 3*d* spin magnetic moments are aligned parallel to that of Ni 3*d* spin in both samples.

Next, we deduced the orbital (m_{orb}) and spin (m_{spin}) magnetic moments per Ni and Fe atom for the samples by applying the sum-rule analysis [31,32]. The background

of the XAS spectra were subtracted by a two-step-function aligned at the peak maxima of L_3 and L_2-edges. The relative height ratio was set to be the branching ratio (L_3/L_2) of the respective XAS spectra. The values were L_3/L_2 = 3.73 (3.46) for Fe $L_{2,3}$-edge and 3.27 (3.90) for Ni $L_{2,3}$-edge in Ni_3FeN ($NiFe_3N$). To find the total number of *d* holes (n_h) of Ni and Fe atoms in the grown films, we referred to the calculated values [16]. The n_h values were 1.36 (1.4) for Ni and 3.48 (3.43) for Fe atoms in Ni_3FeN (Ni_3FeN). As for Ni atoms in Ni_3FeN, we used site-averaged n_h value as described later. We assumed that the effect of the magnetic dipole moment on the spin magnetic moment was negligible as is the case in bcc-Fe and cubic Fe nitride [33]. The m_{orb}, m_{spin}, and total magnetic moment ($m_{tot} = m_{orb} + m_{spin}$) are summarized in Table I. The resulting m_{tot} of Fe atoms was 2.12 ± 0.05 μ_B/Fe for Ni_3FeN and 2.11 ± 0.09 μ_B/Fe for $NiFe_3N$ films. There was a slight difference between these values and those in Fe (i.e., 2.06 μ_B/Fe) and Fe_4N (i.e., 2.15 μ_B/Fe at 5 K) [26,34]. On the other hand, there was a considerable difference in m_{tot} for the Ni atom between the Ni_3FeN and $NiFe_3N$ films; the values were 0.47 ± 0.07 μ_B/Ni and 0.96 ± 0.07 μ_B/Ni, respectively. Here, it should be mentioned that the following approximations which allow us to deduce site-averaged m_{spin} (m_{spin}^{ave}) of Ni atoms for Ni_3FeN in the present case, that is, there are two inequivalent Ni sites in the nitrides lattice (I and II). On the basis of the sum-rules, when there are one Ni atom at I site and two Ni

atoms at II sites, the m_{spin}^{ave} = [m_{spin}(I) + 2m_{spin}(II)]/3 is given by,

$$m_{spin}^{ave} = -\frac{6p(\mathrm{I}) - 4q(\mathrm{I})}{3r(\mathrm{I})} n_h(\mathrm{I}) - 2 \times \frac{6p(\mathrm{II}) - 4q(\mathrm{II})}{3r(\mathrm{II})} n_h(\mathrm{II}) \quad (1)$$

where *p*, *q*, and *r* denote the XMCD integration area of L_3, L_3+L_2, and the integrations of the XAS spectrum above the background, respectively, which are used in Chen *et al*. [34]. Since n_h for the two different sites has been predicted to be almost same by the first-principles calculation [n_h(I) = n_h(II) = n_h] [16], Eq. (1) can be approximated by

$$m_{spin}^{ave} \sim -\frac{6[p(\mathrm{I}) + 2 \times p(\mathrm{II})] - 4[q(\mathrm{I}) + 2 \times q(\mathrm{II})]}{[r(\mathrm{I}) + 2 \times r(\mathrm{II})]} n_h, \quad (2)$$

where, r(I)+2×r(II) = 3r(I) = 3r(II). From Eq. (2), we can obtain m_{spin}^{ave} by using experimentally measured p[q, r](I)+2×p[q, r](II). The background does not affect the final values of magnetic moment significantly. We examined several types of backgrounds with variable different step-height ratios (*see above*), the mean values of magnetic moment were comparable to the error-bar.

In most antiperovskite-type ferromagnetic nitrides, m_{spin} is enhanced at I sites owing to electron localization, whereas m_{spin} is decreased at II sites owing to strong hybridization between the metal 3*d* and N 2*p* orbitals [35]. Therefore, the relatively large value of m_{spin} for Ni atoms in the $NiFe_3N$ film suggests that Ni atoms preferentially occupy I sites, unlike Ni_3FeN films, where Ni atoms are likely to occupy both I and II

sites. Preferential occupation of Ni atom at I site leads to the results that Ni_3FeN tends not to take the state possessing the large spin-polarization. The values of the saturation magnetization calculated from m_{tot} were 620 ± 40 and 1250 ± 50 emu/cm^3 for the Ni_3FeN and $NiFe_3N$ films, respectively.

IV. CONCLUSION

XAS and XMCD measurements of $Ni_xFe_{4-x}N$ (x = 1 and 3) epitaxial films were performed at the $L_{2,3}$ edges of Ni and Fe atoms, and the N K absorption edges. Shoulders were observed at photon energies 2 eV above the main peaks of the Fe $L_{2,3}$-edges in the XAS spectra for both the Ni_3FeN and $NiFe_3N$ films. These features were attributed to orbital hybridization between Fe at II sites and N atoms at body center sites. No such shoulders were observed at the Ni $L_{2,3}$-edges of the $NiFe_3N$ film, whereas these features appeared in a Ni_3FeN film. These results indicate that Ni atoms were not hybridized with N atoms in the $NiFe_3N$ film, and Ni atoms preferentially occupied I sites, which are farther away from the N atoms. The m_{spin} and m_{orb} values were deduced from the obtained XAS and XMCD spectra by sum-rule analysis. The obtained relatively large m_{spin} per Ni atom in the $NiFe_3N$ film also indicated the preferred site occupation of Ni atoms at I sites. The observed XMCD peak at the N K-edges implies that the magnetic moment was

induced at the N atom owing to the hybridization between the transition metal 3*d* and N 2*p* orbitals.

ACKNOWLEDGMENTS

This work was performed under the Shared Use Program of JAEA Facilities (Proposal No. 2017A-E22) with the approval of Nanotechnology Platform project supported by the Ministry of Education, Culture, Sports, Science and Technology (Proposal No. A-17-AE-0020). The synchrotron radiation experiments were performed at JAEA beamline BL23SU in SPring-8 (Proposal No.2017A3842). This work was supported in part by the Center for Spintronics Research Network (CSRN), Tohoku University.

[1] S. Kokado, N. Fujima, K. Harigaya, H. Shimizu, and A. Sakuma, Phys. Rev. B **73**, 172410 (2006).

[2] A. Narahara, K. Ito, T. Suemasu, Y. K. Takahashi, A. Ranajikanth, and K. Hono, Appl. Phys. Lett. **94**, 202502 (2009).

[3] Y. Komasaki, M. Tsunoda, S. Isogami, and M. Takahashi, J. Appl. Phys. **105**, 07C928 (2009).

[4] Y. Takahashi, Y. Imai, and T. Kumagai, J. Magn. Magn. Mater. **323**, 2941 (2011).

[5] T. Sanai, K. Ito, K. Toko, and T. Suemasu, J. Cryst. Growth **378**, 342 (2013).

[6] H. Sakakibara, H. Ando, T. Miyawaki, K. Ueda, and H. Asano, IEEE Trans. Magn. **50**, 2600404 (2014).

[7] K. Ito, K. Kabara, T. Sanai, K. Toko, Y. Imai, M. Tsunoda, and T. Suemasu, J. Appl. Phys. **116**, 053912 (2014).

[8] K. Ito, T. Sanai, Y. Yasutomi, T. Gushi, K. Toko, H. Yanagihara, M. Tsunoda, E. Kita, and T. Suemasu, J. Appl. Phys. **117**, 17B717 (2015).

[9] S. K. Chen, S. Jin, T. H. Tiefel, Y. F. Hsieh, E. M. Gyorgy, and D. W. Johnson Jr., J. Appl. Phys. **70**, 6247 (1991).

[10] M. Kume, T. Tsujioka, K. Matsuura, and Y. Abe, IEEE Trans. Magn. **MAG-23**, 3633 (1987).

[11] G. Shirane, W. J. Takei, and S. L. Ruby, Phys. Rev. **126**, 49 (1962).

[12] F. Li, J. Yang, D. Xue, and R. Zhou, Appl. Phys. Lett. **66**, 2343 (1995).

[13] X. G. Diao, A. Y. Takeuchi, F. Garcia, R.B. Scorzelli, and H. R. Rechenberg, J. Appl. Phys. **85**, 4485 (1999).

[14] R. J. Arnott and A. Wold, J. Phys. Chem. Solids **15**, 152 (1959).

[15] R. Loloee, J. Appl. Phys. **112**, 023902 (2012).

[16] Y. Kong and F. Li, Phys. Rev. B **57**, 970 (1998).

[17] P. Mohn, K. Schwarz, S. Matar, and G. Demazeau, Phys. Rev. B **45**, 4000 (1992).

[18] Y. Q. Wu and M. F. Yan, Physica B **405**, 2700 (2010).

[19] P. Monachesi, T. Björkman, T. Gasche, and O. Eriksson, Phys. Rev. B **88**, 054420 (2013).

[20] F. Takata, K. Ito, S. Higashikozono, T. Gushi, K. Toko, and T. Suemasu, J. Appl. Phys. **120**, 083907 (2016).

[21] K. Kabara, M. Tsunoda, and S. Kokado, Appl. Phys. Express **7**, 063003 (2014).

[22] F. Takata, K. Kabara, K. Ito, M. Tsunoda, and T. Suemasu, J. Appl. Phys. **121**, 023903 (2017).

[23] K. Ito, T. Sanai, S. Zhu, Y. Yasutomi, K. Toko, S. Honda, S. Ueda, Y. Takeda, Y. Saitoh, Y. Imai, A. Kimura, and T. Suemasu, Appl. Phys. Lett. **103**, 232403 (2013).

[24] K. Ito, T. Sanai, Y. Yasutomi, S. Zhu, K. Toko, Y. Takeda, Y. Saitoh, A. Kimura, and T. Suemasu, J. Appl. Phys. **115**, 17C712 (2014).

[25] K. Ito, K. Toko, Y. Takeda, Y. Saitoh, T. Oguchi, T. Suemasu, and A. Kimura, J. Appl. Phys. **117**, 193906 (2015).

[26] Y. Takagi, K. Isami, I. Yamamoto, T. Nakagawa, and T. Yokoyama, Phys. Rev. B **81**, 035422 (2010).

[27] Y. Saitoh, Y. Fukuda, Y. Takeda, H. Yamagami, S. Takahashi, Y. Asano, T. Hara, K. Shirasawa, M. Takeuchi, T. Tanaka, and H. Kitamura, J. Synchrotron Radiat. **19**, 388 (2012).

[28] C. T. Chen, F. Sette, Y. Ma, and S. Modesti, Phys. Rev. B **42**, 7262 (1990).

[29] N. V. Smith, C. T. Chen, F. Sette, and L. F. Mattheiss, Phys. Rev. B **46**, 1023 (1992).

[30] T. Jo and G. A. Sawatzky, Phys. Rev. B **43**, 8771 (1991).

[31] B. T. Thole, P. Carra, F. Sette, and G. van der Laan, Phys. Rev. Lett. **68**, 1943 (1992).

[32] P. Carra, B. T. Thole, M. Altarelli, and X. D. Wang, Phys. Rev. Lett. **70**, 694 (1993).

[33] M. Alouani, J. M. Wills, and J. W. Wilkins, Phys. Rev. B **57**, 9502 (1998).

[34] C. T. Chen, Y. U. Idzerda, H. -J. Lin, N. V. Smith, G. Meigs, E. Chaban, G. H. Ho, E. Pellegrin, and F. Sette, Phys. Rev. Lett. **75**, 152 (1995).

[35] X. G. Ma, J. J. Jiang, P. Liang, J. Wang, Q. Ma, and Q. K. Zhang, J. Alloys Compd.

480, 475 (2009).

TABLE I. Obtained m_{orb}, m_{spin}, and m_{tot} values for Ni and Fe atoms in Ni_3FeN and $NiFe_3N$.

Compounds	Atom	Magnetic moment [μ_B/atom]		
		m_{orb}	m_{spin}	m_{tot}
Ni_3FeN	Ni (100 K)	0.06 ± 0.01	0.41 ± 0.06	0.47 ± 0.07
	Fe (100 K)	0.05 ± 0.01	2.07 ± 0.05	2.12 ± 0.05
$NiFe_3N$	Ni (100 K)	0.09 ± 0.01	0.87 ± 0.07	0.96 ± 0.07
	Fe (100 K)	0.07 ± 0.02	2.04 ± 0.08	2.11 ± 0.09

Figure captions

FIG. 1. Crystalline structure of antiperovskite-type transition metal nitrides. Face-centered II sites can be further divided into IIA and IIB sites with magnetization. Without magnetization, Fe-IIA and Fe-IIB are equivalent.

FIG. 2. XAS and XMCD spectra in (a) Ni_3FeN and (b) $NiFe_3N$ films at Ni-$L_{2,3}$ edges.

FIG. 3. XAS and XMCD spectra in (a) Ni_3FeN and (b) $NiFe_3N$ films at Fe-$L_{2,3}$ edges.

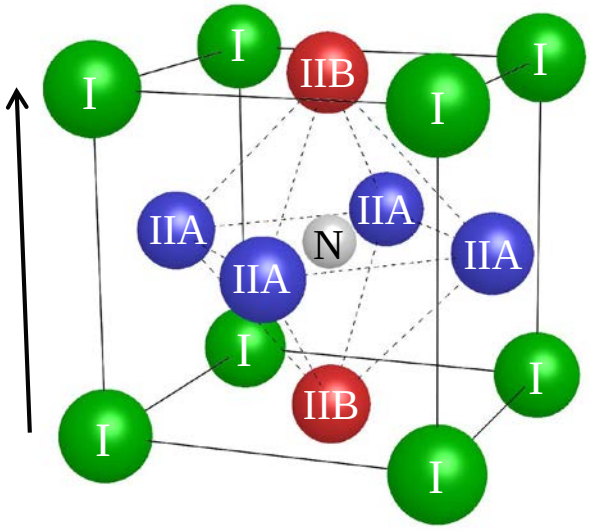

FIG. 1.

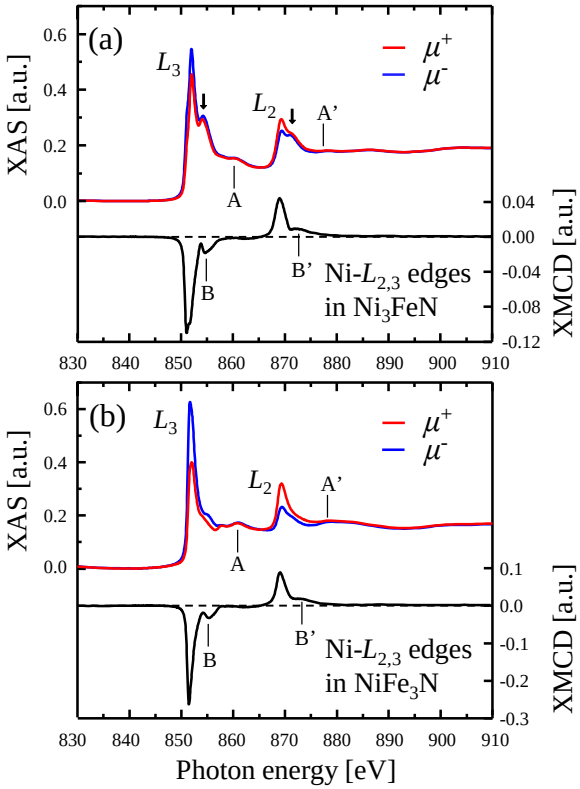
(a)
L_3
L_2
A'
A
B'
B
μ^+
μ^-
Ni-$L_{2,3}$ edges
in Ni_3FeN
XAS [a.u.]
XMCD [a.u.]
(b)
L_3
L_2
A'
A
B'
B
μ^+
μ^-
Ni-$L_{2,3}$ edges
in $NiFe_3N$
XAS [a.u.]
XMCD [a.u.]
Photon energy [eV]

FIG. 2.

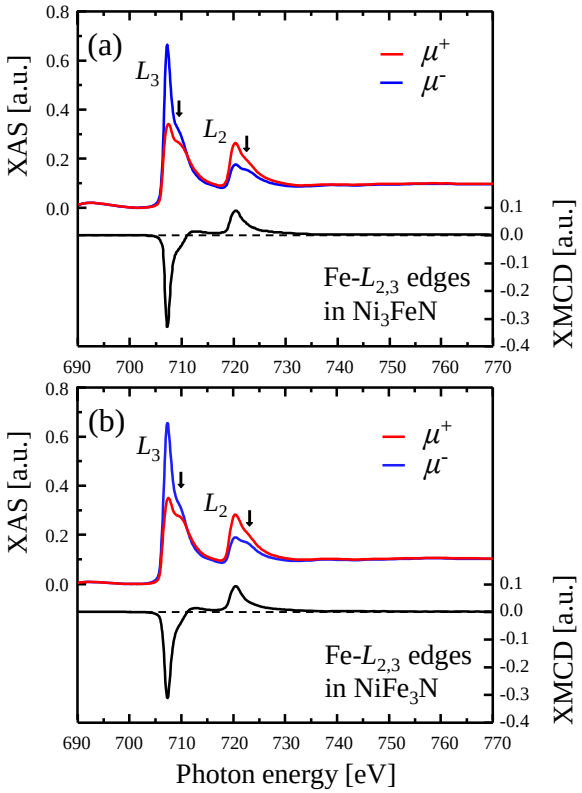
(a)
L_3
L_2
μ^+
μ^-
Fe-$L_{2,3}$ edges
in Ni_3FeN
XAS [a.u.]
XMCD [a.u.]
(b)
L_3
L_2
μ^+
μ^-
Fe-$L_{2,3}$ edges
in $NiFe_3N$
XAS [a.u.]
XMCD [a.u.]
Photon energy [eV]

FIG. 3.